



www.cerf-jcr.org

Video-Based Detection of Shorelines at Complex Meso–Macro Tidal Beaches

Rafael Almar^{†‡}, Roshanka Ranasinghe^{§††}, Nadia Sénéchal[†], Philippe Bonneton[†],
Dano Roelvink^{††}, Karin R. Bryan^{‡‡}, Vincent Marieu[†], and Jean-Paul Parisot[†]

[†]Université Bordeaux 1
CNRS, UMR 5805 EPOC
Avenue des Facultés
33405 Talence, France

[‡]Pontificia Universidad Católica de Chile
Escuela de Ingeniería
Av. Vicuña Mackenna 4860
Macul, Santiago, Chile
ralmar@ing.puc.cl

[§]Department of Civil Engineering and
GeoSciences (CiTG)
Delft University of Technology
P.O. Box 5048
2600 GA Delft, The Netherlands

^{††}Department of Water Engineering
UNESCO-IHE
P.O. Box 3015
2601 DA Delft, The Netherlands

^{‡‡}Department of Earth and Ocean Sciences
University of Waikato
Private Bag 3105
Hamilton, 3240, New Zealand

ABSTRACT

Almar, R.; Ranasinghe, R.; Sénéchal, N.; Bonneton, P.; Roelvink, D.; Bryan, K.R.; Marieu, V., and Parisot, J-P., 2012. Video-based detection of shorelines at complex meso–macro tidal beaches. *Journal of Coastal Research*, 28(5), 1040–1048. Coconut Creek (Florida), ISSN 0749-0208.

Remote video imagery is widely used to acquire measurements of intertidal topography by means of shoreline detection, but, up to now, problems of accuracy were still encountered in the challenging case of energetic waves in nonuniform, meso–macro tidal environments. Unique, simultaneous, video-based and global positioning system (GPS)–based measurements of shoreline were undertaken at Truc Vert (France), a beach with such characteristics. An innovative video method, referred to herein as the Minimum Shoreline Variability (MSV) method, was developed to cope with highly variable spatiotemporal shoreline properties. The comparison of video-based and GPS-derived shoreline data sets showed that using images averaged over short periods (30 s), rather than the traditionally used 10-min averaged images, significantly improved the accuracy of shoreline determination. A local video-derived, swash-based shoreline correction was also developed to correct for the MSV error, which was found to be linearly correlated to local swash length. By combining shorter time-averaged images and video derived local swash correction factors, the horizontal root mean square error associated with MSV shorelines was reduced to 1.2 m, which is equivalent to errors reported at more uniform, microtidal, and less-energetic beaches.

ADDITIONAL INDEX WORDS: *Video imaging, shoreline, swash, intertidal beach morphology, meso–macro tidal environment, Truc Vert beach.*



www.JCRonline.org

INTRODUCTION

The shoreline is often adopted as an indicator of both short- and long-term coastline changes that are central to defining the coastal hazard zone. Despite its common usage, the shoreline has been given several definitions based on different approaches: physical, geological, biological, or coastal engineering. Boak and Turner (2005) describe a wide variety of shoreline definitions. Depending on the definition, the shoreline position can vary up to hundreds of meters. The choice of the period over which the waterline is averaged to determine the shoreline will also cause some differences between shoreline definitions.

Video-based remote sensing is particularly well suited to shoreline monitoring because it covers timescales from seconds to years and spatial scales from meters to kilometres. Numerous video studies have gone into estimating shoreline

position. The main applications are in assessing natural beach behaviour (Davidson *et al.*, 2007; Smit *et al.*, 2007), artificial nourishment efficiency (Castelle *et al.*, 2009; Kroon *et al.*, 2007), and beaches dedicated to recreational use and safety (Jiménez *et al.*, 2007). Video-detected shorelines are commonly estimated using time-exposure images (Aarninkhof *et al.*, 2003; Holman and Stanley, 2007; Rihouey *et al.*, 2009; Silva *et al.*, 2009). The aim is to smooth out high-frequency signals that are caused by individual waves and foam motion and to isolate a mean shoreline position. Ten-minute averaging is commonly used (Plant *et al.*, 2007) because that filters out the most common incident and high-frequency, nearshore hydrodynamic components. Different proxies have been used for identifying the shoreline from such time-averaged video images. Plant and Holman (1997) used a method initially developed for grayscale cameras, called the Shore Line Intensity Maximum (SLIM). The SLIM method defines the shoreline as the cross-shore position at which wave breaking is maximized, which corresponds to a maximum in pixel intensity close to the shore. Although accurate for an alongshore, uniform topography,

DOI: 10.2112/JCOASTRES-D-10-00149.1 received 1 October 2010; accepted in revision 4 February 2011.

© Coastal Education & Research Foundation 2012

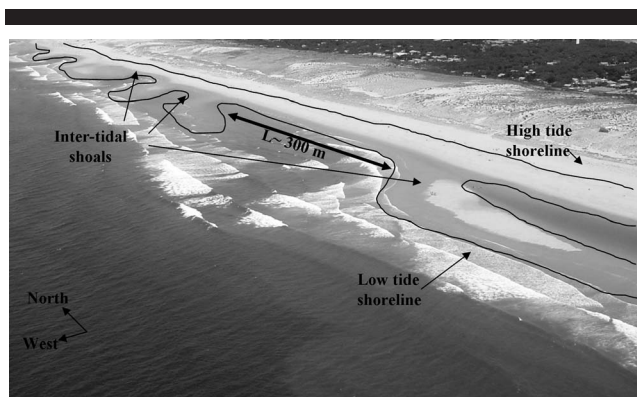


Figure 1. A typical Aquitanian coast beach (Cap Ferret, France) located in a meso–macro tidal environment. The intertidal area is wide with a ridge and runnel system containing large shoals and troughs. This type of morphology presents significant challenges for video shoreline detection. The black line delineates the approximate location of the shoreline.

problems arise for complex shorelines that do not necessarily have a shore break (*i.e.*, beaches with bar and rip topography). With the adoption of colour cameras in nearshore monitoring systems, spectral information could also be used to identify the shoreline. These methods make use of the water property of absorbing the red signal to differentiate between land and water; *i.e.*, image pixels associated with a minimum in the red channel and maxima in the green and blue channels are taken as water pixels, whereas pixels associated with a maximum in the red channel and minima in the green and blue channels are taken as beach pixels. The shoreline is then defined as the transition zone between beach pixels and water pixels and is expected to correspond to the limit between water and sand (Bryan, Smith, Ovenden, 2003; Smith and Bryan, 2007; Turner *et al.*, 2001). Turner *et al.* (2001) also developed the Channel Colour Divergence (CDD) method based on red, green, and blue channels having similar values on the white sand of the beach but having different values in the water. The shoreline is defined on each cross-shore transect where divergence between colour channels exceeds a certain threshold. A Pixel Intensity Clustering (PIC) technique was developed by Aarninkhof *et al.* (2003) that uses both colour information and grayscale intensity.

All these methods were developed and tested successfully for relatively uncomplicated coastal areas that were mostly located in microtidal environments with moderate wave conditions. However, those methods fail to robustly and accurately determine the shoreline at beaches with high wave energy and meso–macro tidal environments with high temporal and spatial variability. Such beaches consist of shoals and channels that emerge and submerge quite rapidly because of the large tidal range. Although these types of beaches can be found around the world, the southern French coastline is a good example of a coastline that contains many such beaches (Figure 1).

This article presents a new video-based method (including a local swash-based correction) designed specifically to robustly and accurately determine shorelines at complex meso–macro

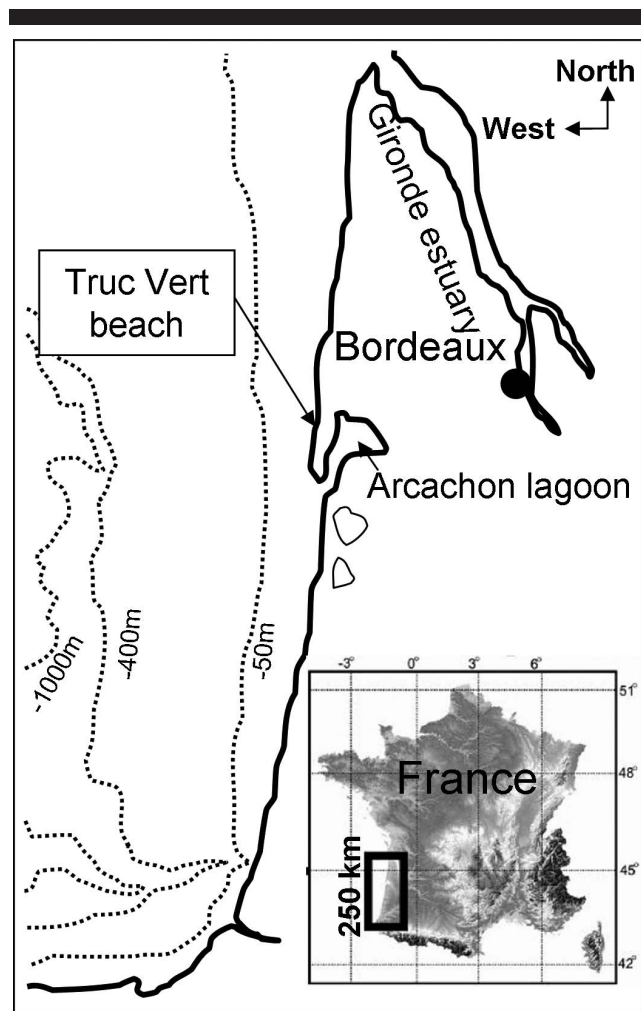


Figure 2. Location of Truc Vert beach (Aquitanian coast, southwestern France).

tidal, high wave-energy beaches with nonmonotonic shorelines. The method was validated with data acquired in a field experiment at a typical meso–macro tidal, high-energy beach located along the French Aquitanian coast: Truc Vert beach.

METHODS

Study Area

The Truc Vert beach is located on the straight sandy Aquitanian Coast, 20 km to the north of the Arcachon Lagoon entrance, in southwestern France (Figure 2). Incident waves are mainly from the WNW and the wave-climate is characterized by a 1.4-m mean annual significant wave height (H_s) and a 6.5 s peak-wave period (Butel, Dupuis, Bonneton, 2002). The meso–macro tidal signal in the area is semidiurnal with spring and neap tidal ranges of 5 m and 2 m, respectively. The beach slope is 0.03. The sediment consists of fine to medium quartz sand with median-grain sizes ranging from 200 to 400 μm (Pedreros, Howa, Michel, 1996). The beach is mainly intermediate and double-barred according to the beach state classification of Wright and Short (1984) and consists of a

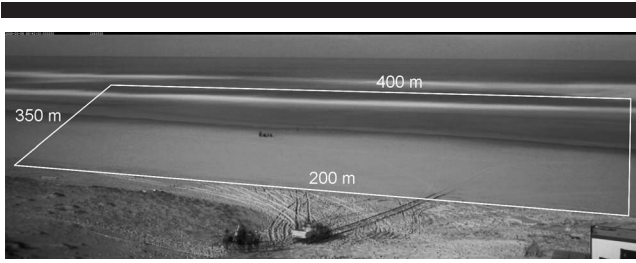


Figure 3. Time-exposure oblique image from the Truc Vert beach (France) temporary video system. Our region of interest (ROI) is delimited in white.

rhythmic outer bar and a highly variable inner bar (Castelle *et al.*, 2007). The inner bar, which is located in the intertidal zone, commonly exhibits a transverse bar and rip (TBR) morphology with a mean wavelength of about 400 m (Lafon *et al.*, 2002). Because of the meso–macro tidal range, the beach consists of a large and complex intertidal area (see intertidal morphology in Figure 1).

ECORS Field Experiment

The ECORS field experiment was undertaken at Truc Vert beach (SW France) from 1 March 2008 to 9 April 2008. The aim of the experiment was to study short-term beach response to storms (for more details see Sénéchal and Ardhuin, 2008). During the experiment, the Aquitanian coast experienced energetic wave conditions with spring tidal conditions. Several high-frequency hydrodynamic and morphological measurements were undertaken during the experiment. Of these, the present study focuses only on the video-imaging data and time-varying shoreline data obtained by global positioning system (GPS) trackers.

Video Imaging

A video-imaging system (Organisation for Economic Co-operation and Development [OECD] Environnements et Paléoenvironnements Océaniques [EPOC; France]–New Zealand National Institute of Water and Atmospheric [NIWA]; Coco, Bryan, and Payne, 2004) was deployed during the experiment (Almar *et al.*, 2010). Cameras were mounted on an 8-m-high scaffolding situated on top of the dune, which resulted in a total camera elevation of 27 m above mean sea level. The system consisted of two high-resolution cameras (3.5 megapixels) covering an alongshore distance of 1.5 km and a cross-shore distance of 1 km. Data acquisition was continuous (at 2 Hz sampling frequency) during daylight hours. Using these snapshot images allowed the generation of 0.5-, 2-, and 10-min time-exposure images to investigate the optimal image-averaging time for shoreline detection. Rectification of images from pixel coordinates into real-world coordinates (Holland *et al.*, 1997) was accomplished using differential GPS (DGPS) ground-survey points (centimetre precision). Because of the oblique camera angle, the pixel resolution at the image lateral edges is about 0.5 m, whereas it is about 0.1 m at the lower beach in front of the video system. Comparison between estimated and ground-surveyed point positions indicates an accuracy of about 1 m and 0.3 m, respectively, at the image lateral edges and at the lower beach in front of the video system.

Video Detection of the Shoreline

As discussed above, existing video shoreline-detecting techniques are not particularly appropriate for the complex, nonmonotonic shorelines with high temporal and spatial variabilities that are commonly found in meso–macro tidal environments. Therefore, the objective was to develop a robust technique that is suited specifically for such coastal areas. The two-step approach adopted in this study to achieve this objective combines two intrinsic shoreline properties: (1) the colour difference between water and sand (as in past work), and (2) the presence of swash (not necessarily breaking). The method, which is described below, is, by necessity, two-dimensional to accommodate the complex morphology.

Step 1: Determination of Shoreline Colour Ratio and Assessment of Image Quality. Following existing methods, a region of interest (ROI) is defined in the oblique images to cover both wet and dry pixels (Figure 3). The method is based on three-banded red–green–blue (RGB) images and on the behavioural difference among the intensities of the three colour channels in water and on dry beach. Beach pixels usually exhibit high red-channel values and low green-channel values (*i.e.*, high $R:G$ ratio), whereas water pixels exhibit intense green-channel values and low red-channel values (*i.e.*, low $R:G$ ratio). The $R:G$ ratios are thus computed for all pixels within the ROI. A histogram is then generated, representing the number of pixels for each $R:G$ bin (bin size ≈ 0.001). The histogram generally shows a bimodal distribution (Figure 4b, middle panel) where the lower and higher $R:G$ peaks are expected to be associated with water and beach, respectively. The local minimum, *i.e.*, the transition zone between the two peaks, then represents the shoreline. For some conditions, however, the histogram is not strictly bimodal, with more than one minimum being present (Figure 4a, middle panel). For example, this can be the case at low tide when the lower beach is wet because of the groundwater table exit point being higher than the shoreline. Under these circumstances, the sand characteristics of the wet lower beach are different than those of the dry upper beach. In such cases, pixels that are relatively close together are grouped to produce two main groups of pixels (an example is shown in Figure 4a), which are then taken to represent water and beach as a first approximation.

An iterative method for low-pass band clustering of the $R:G$ histograms was, therefore, developed with the primary aim of ensuring the robust, automatic determination of the two main $R:G$ peaks. Image quality assessment is based on the physical consideration that the colour contrast between beach and water is sufficient, lighting is strong enough, and the numbers of pixels in the water and beach groups are sufficient to be representative of colour characteristics in these zones. In this method, the histogram is first severely smoothed, and then, the smoothing is iteratively decreased until the following conditions are satisfied:

- (1) Exactly two significant peaks are present
- (2) Local minimum is well pronounced
- (3) Lighting is sufficient (*i.e.*, beach peak $R:G > 0.9$)

If these conditions are satisfied, the local minimum of the resulting histogram is taken as a first estimate of the shoreline

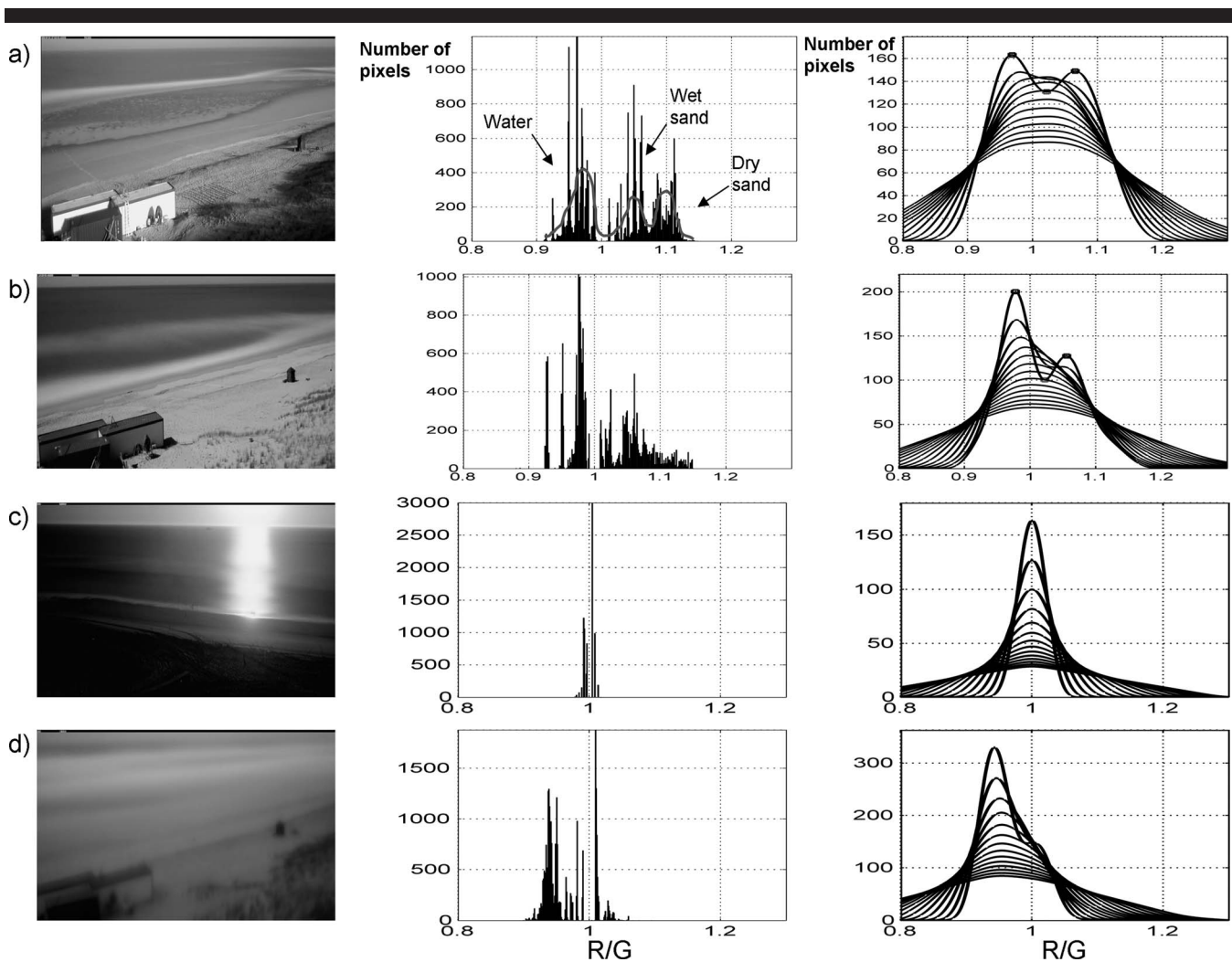


Figure 4. Image quality and initial shoreline determination. Original video image (left), histogram of colour ratios (centre), and iterative method (right), where each line represents a progressive smoothing of the histogram. (a) Low tide and sunny weather: image accepted. (b) High tide and sunny weather: image accepted. (c) High tide with sun glint: image rejected. (d) Foggy conditions: image rejected.

$R : G$ value (Figures 4a and b). If, however, the above conditions are not satisfied, the image is rejected. Rejected images can be classified into two classes. In the first class, a group of pixels dominates the image signal (sun glint or fog, see Figures 4c and d), which results in a unique peak. In the second class, the images are under exposed (e.g., in the morning or evening) resulting in a beach peak with $R : G < 0.9$.

Step 2: Shoreline Position. The second step of our method is the detection of the shoreline position. This is based on the physical fact that swash (incident or infragravity) is always present at the shoreline, regardless the complexity of the topography and the local occurrence of breaking (Ruessink, 1998). The shoreline is detected using the swash signature on time-averaged video images. In terms of video detection, it is reasonably assumed that two close contours of $R : G$ values at the shoreline have similar shapes. In this step of the newly developed shoreline-detection method, several contour lengths

(L) are computed for different $R : G$ values around the local minimum identified in step 1. The local minimum of $\Delta L / L$ for varying $R : G$ is used to infer the associated value of $R : G_{Shoreline}$ and thus the contour position (x, y) (Equation 1). The L depends on the ROI width and its variation ΔL is typically in the order of 1 to 30% of L .

This estimate is taken as the shoreline position $(x, y)_{Shoreline}$ corresponding to the swash-averaged position:

$$\min \left(\frac{\Delta L_i}{L_i} \right)_{i=R:G_1 : R:G_2} \Rightarrow R : G_{Shoreline} \stackrel{\text{contour position}}{\Rightarrow} (x, y)_{Shoreline} \quad (1)$$

with $R : G_1$ and $R : G_2$ being iteration boundaries around the step 1 estimation.

Figures 5a and b illustrate the application of this method for a high-tide, alongshore-uniform topography and for a complex, low-tide topography, respectively. The value of $\Delta L / L$ for varying $R : G$ is plotted in the lower panels. Minima are associated with detected swash-averaged smooth shorelines,

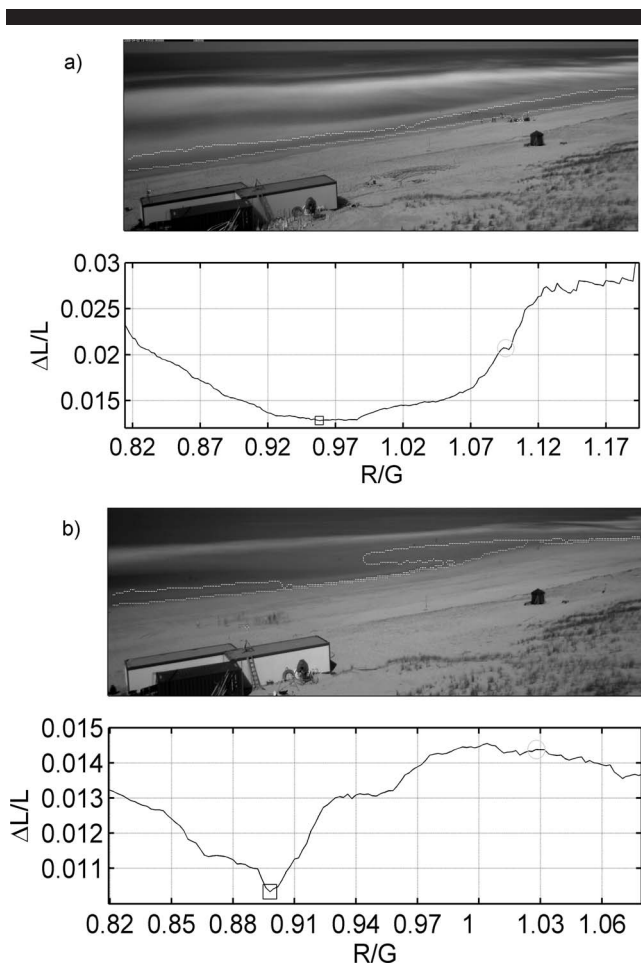


Figure 5. The MSV method test cases for conditions presented in (a) Figure 4a and (b) Figure 4b, respectively. Top panels show the resulting shoreline position. Bottom panels show the length variation of the shoreline ($\Delta L/L$) for varying $R:G$ values. The squares indicate the minimum variation. The circles indicate the $R:G$ value associated with the first estimated shoreline.

rather than with dry/wet sand limits, which present a noisy contour and a larger $\Delta L/L$ value. In the two cases shown in Figures 5a and b, the first estimated shorelines (step 1) do not necessarily correspond with the water/sand boundary, whereas the refined estimated shorelines (step 2) correspond well with

that boundary. Unlike most previous video shoreline-detection methods, which required a further manual check (Uunka, Wijnberg, and Morelissen, 2009), the method developed here has the ability to differentiate between the water/land boundary (smooth) and the dry sand/wet sand boundary (sharp), and to preferentially pick the former as the shoreline.

The shoreline thus identified on the oblique image is converted to real-world coordinates using standard image-rectification techniques. Finally, shorelines obtained from corresponding images from the two cameras are merged to form a continuous shoreline. For convenience, the above method is referred to as the MSV (Minimum Shoreline Variability) method hereafter.

GPS Tracking of Shoreline

The GPS measurements of the shoreline were undertaken at Truc Vert, France, to assess the performance of the newly developed MSV method under various wave and tide conditions. The shoreline position was tracked intensively by 10 field assistants using handheld GPS, both in the alongshore and cross-shore directions. The GPS tracks were acquired between the 2 April 2008 and 4 April 2008 under various tidal and wave conditions (see Table 1). Whereas video-image rectification was done using a real-time kinematic (RTK) GPS (Trimble 5700, centimetre precision), rapid shoreline tracks were performed with a handheld Garmin 12 GPS, which showed a 2-m precision when tested in the field (Parisot *et al.*, 2009).

To obtain alongshore tracks of the shoreline, several field assistants carrying GPS receivers followed the visually detected water–sand interface (average between swashes). The alongshore distance covered in each track was approximately 400 m. The individual tracks spanned durations between 2 and 3 min and were collected consecutively. Seven separate groups of shorelines, taken at different stages of the tide, each consisting of five to seven individual tracks, were obtained (Table 1). The first track of each group is shown in Figure 6.

To determine the cross-shore location of the time-averaged MSV shoreline position with high accuracy, so that the MSV shorelines could be validated, GPS tracks were also obtained in the cross-shore direction at four alongshore locations (indicated in Figure 6 by thick yellow arrows). Here, the GPS trackers followed the cross-shore movement of swash over a 20-min period. The swash tracks were strategically performed to cover a range of hydrodynamic conditions and morphological fea-

Table 1. Description of alongshore GPS tracks.

Alongshore Track Group No.	No. of Tracks	Mean Slope	Hydrodynamic Conditions		Comments
			Tide	H_s (m)	
1	7	0.029	Mid	2.5	Flat, almost uniform
2	7	0.034	Mid	2.2	
3	5	0.039	Mid-high	2.2	
4	4	0.043	High	2.1	Upper beach
5	7	0.060	High	2.0	Upper beach
6	5	0.009	Low	2.0	Emerging shoals
7	5	0.013	Low	1.7	Emerged shoals

Abbreviation: H_s = significant wave height.

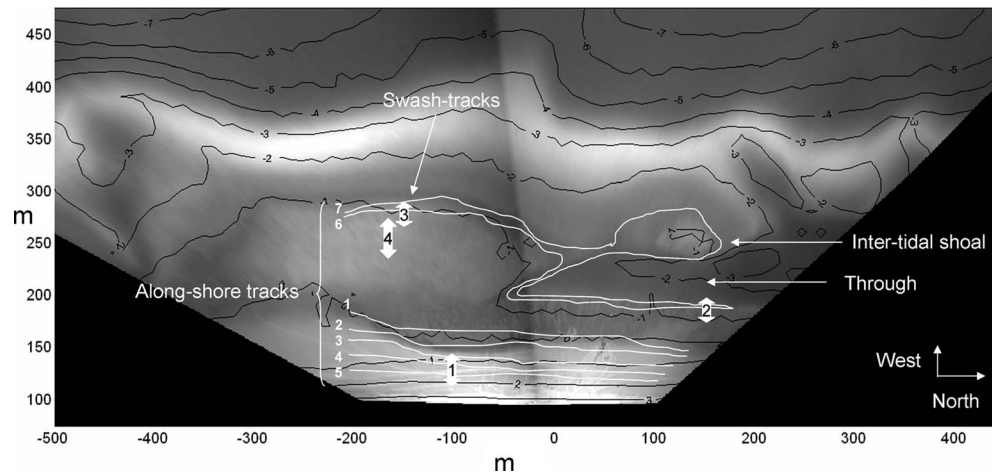


Figure 6. The GPS tracks (white lines) superimposed on a rectified, time-exposure image. Double-headed arrows indicate cross-shore GPS swash tracks. See Tables 1 and 2 for further description of the GPS tracks. Black lines are depth contours from a concurrent hydrographic survey.

tures as indicated in Table 2. An accurate estimation of shoreline position was thus computed by averaging 20-min swash-tracked time series. The rationale used in this study was that GPS-based shoreline and swash data are the most accurate, and thus video-derived data can be verified and/or corrected using the GPS data.

RESULTS AND DISCUSSION

Sensitivity to Image-Averaging Time

Alongshore GPS tracks were performed to cover the entire intertidal area during a tidal cycle and ranged between 250 and 600 m in length (see Figure 6). The variability of individual alongshore GPS trackings revealed the subjectivity associated with a visual definition of the shoreline position. To minimize this human-induced variability, representative shorelines were obtained by averaging the four to six consecutive tracks obtained within each of the seven groups of alongshore trackings (note: each group's tracking spanned approximately 10 min). Corresponding groups of consecutive MSV shorelines were then obtained from 10-, 2-, and 0.5-min time-exposure images. These were averaged over time spans that were

concurrent with GPS group observations to allow a fair comparison.

The sensitivity of the MSV method to video image-averaging time was investigated by calculating the percentage occurrence of the differences between the GPS and MSV shorelines. The cross-shore differences between the GPS and MSV shorelines were calculated by subtracting the MSV positions from the GPS ones (after linearly interpolating both shorelines into a common sampling interval).

The overall percentage of difference occurred between GPS data thus calculated is shown in Figure 7 and indicates a Gaussian distributions centred on -5.6 m and -3.3 m (*i.e.*, on average, MSV being slightly seaward of the GPS) for 10-min and 0.5-min averaged video images, respectively. The high and thin peak of the MSV 0.5-min line indicates that the 0.5-min averaged shoreline is more likely to represent the GPS-shoreline than the 10-min averaged shoreline. Mean root mean square (RMS) cross-shore difference between the MSV method and the GPS-obtained shoreline positions were 9.7 m, 8.1 m, and 7.7 m for 10-min, 2-min, and 0.5-min time-exposure images, respectively. This represents a reduction of 19.7% in the GPS/MSV shoreline discrepancy when using 0.5-min

Table 2. Description of cross-shore GPS tracks.

Swash Track No.	Morphological Feature	Local Beach Slope	Hydrodynamic Condition		Comment
			Tide	H_s (m)	
1	Upper beach	0.058	High	2.2	
2	Feeder channel	0.020	Low	1.6	Simultaneously with track 3
3	Seaward face of transverse shoal	0.018	Low	1.6	Simultaneously with track 2
4	Flat area of transverse shoal	0.012	Low, rising	1.5	In conjunction with an intensive short distance (100 m) alongshore tracking (14 trackings with 1 every minute) centred on the cross-shore track

Abbreviation: GPS = global positioning system; H_s = significant wave height.

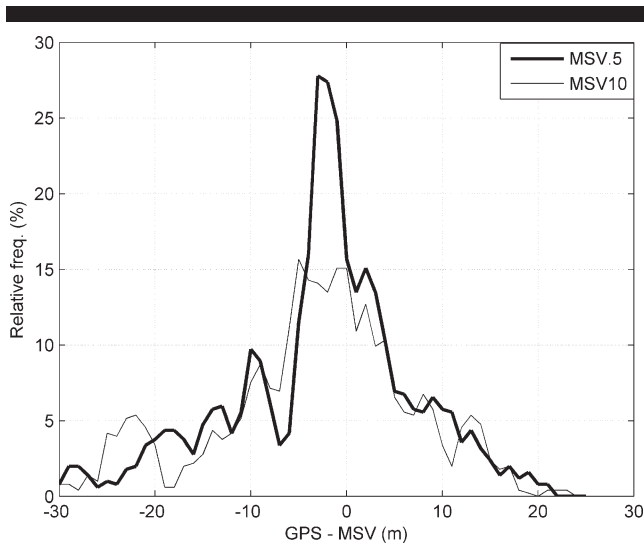


Figure 7. Percentage of occurrence of the GPS–MSV difference for overall shorelines. The thick and thin solid lines indicate percentage of occurrences associated with MSV method shorelines obtained from 0.5-min and 10-min averaged video images, respectively. Negative values of GPS–MSV are obtained when the MSV shoreline is seaward of the GPS shoreline.

averaged images in comparison to the more commonly used 10-min averaged images.

The local accuracy of the MSV method's shorelines was also evaluated taking swash processes into consideration. The GPS-based swash tracks were compared with the corresponding MSV cross-shore positions obtained from 0.5-min, 2-min, and 10-min averaged images (Figure 8). The comparisons were conducted over the GPS swash-track durations, which were approximately 20 min. To compare average cross-shore positions of the shoreline, both the GPS and MSV methods' shoreline positions were detrended to remove the tidal component of shoreline variation (component indicated by straight solid lines in the subplots of Figure 8). Mean RMS deviations between the MSV method and GPS obtained cross-shore shoreline positions are 2.1 m, 1.3 m, and 5.7 m for 0.5-min, 2-min, and 10-min averaged images, respectively (see Table 3). This reiterates the result highlighted previously that shoreline positions obtained by shorter averaging timescales (up to 2 min) are likely to be more accurate.

In particular, a maximum trend of 1 m/min due to tide is indicated in the shoreline position signal (flat beach part, track 4), implying that, in this environment with a large tidal range, nonswash-related time-varying shoreline characteristics are quite likely to be smoothed out when using video images averaged over longer time durations (*e.g.*, 10 m uncertainty for 10-min averaged images). Moreover, GPS swash data indicate the presence of a substantial infragravity component of more than 10 m length attributed to large wave conditions and complex topography. These cumulative effects of large tidal range and large wave conditions can result in a smoothing of shoreline characteristics, resulting in significant errors in shorelines detected using longer time-averaged images.

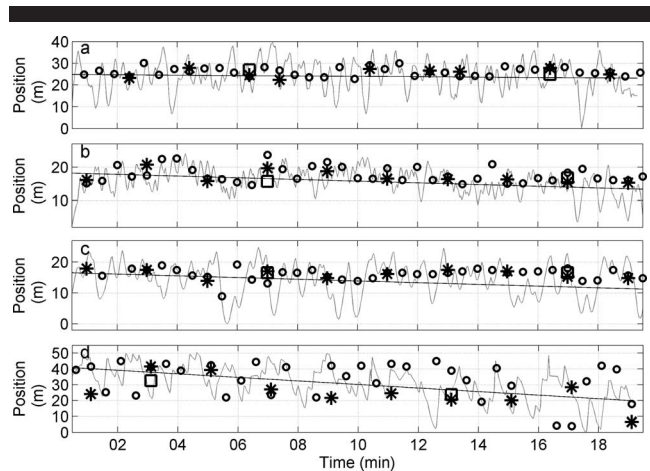


Figure 8. Time series of cross-shore shoreline position. The GPS swash tracks are plotted as solid black lines, and the straight line represents the tidal trend. The circles, squares, and crosses represent the MSV shoreline positions obtained from 0.5-, 2-, and 10-min averaged images: (a) Track 1 (high tide), (b) Track 2 (low tide), (c) Track 3 (low tide), and (d) Track 4 (low tide). See Table 2 for a description of the various GPS tracks.

Error Dependence on Local Swash Length

The video-estimated cross-shore position of the shoreline is within the swash length identified by GPS tracking at all four locations (Figure 8). The estimate is better in steeper areas (swash tracks 1 and 2; Table 2) than in flatter and wave-exposed areas (swash tracks 3 and 4), suggesting a relationship between error and swash length. This relationship was verified using data, in particular, using accurate 0.5-min MSV shoreline data. The differences between MSV shorelines and GPS shoreline positions (both averaged over the same time, 10 min) are plotted as a function of GPS-derived average swash length (L_{sw}) for the four cross-shore tracks (Figure 9). This clearly shows that for 0.5-min averaged images, the difference in the two estimates increases linearly and positively with swash length and indicates that the MSV shoreline positions are 15% (zero-constrained $R^2 > 0.9$) of the swash length seaward of the GPS shoreline positions.

Following Plant *et al.* (2007), we propose a correction for this predictable error based on swash length. The gradient of the line of best fit indicates the correction needs to be applied to the MSV method-derived shoreline positions. In contrast to obtaining a correction factor using data obtained at one location at one time, the inclusion of the four different cross-shore tracks, which were strategically selected to account for both temporal variability in hydrodynamic forcing and temporal/spatial variability in the shoreline, ensures that the correction derived using this technique is more likely to be valid along the entire shoreline at all tidal stages.

The comparison of simultaneous GPS swash measurements at different locations showed that swash was both temporally and spatially variable, indicating the need for a local swash estimation, uniquely possible using video images. Thus, a fully video-based local correction was estimated for the seven GPS shoreline groups (described in Table 1) using MSV L_{sw} estimates on 2 Hz snapshots over a 5-min period. The L_{sw}

Table 3. Comparison of shoreline positions determined by the MSV method and by GPS-tracked cross-shore. Mean RMS error is the mean value over the four cases, and bold values are the RMS error after applying the swash-correction factor.

Swash Track No.	L_{sw} (GPS)	L_{sw} (MSV)	MSV-GPS (0.5 min)	MSV-GPS (2 min)	MSV-GPS (10 min)
1	13.4	13.9	1.9	0.9	3.8
2	8.1	7.3	1.3	0.9	-6
3	11.7	13.8	2	-1	-6.6
4	22.1	20.7	3.3	2.8	6.5
Mean RMS Error (Corrected)		1.2	2.1 (0.1)	1.3 (1.2)	5.7 (5.1)

Abbreviation: GPS = global positioning system; H_s = significant wave height; L_{sw} = average swash length; MSV = Minimum Shoreline Variability method; RMS = root mean square.

values obtained from the MSV were compared with the corresponding GPS-based L_{sw} values at the four cross-shore track locations (Table 3). For the four distinct positions, the mean RMS difference between the L_{sw} obtained using the two methods was an acceptable 1.2 m (8.7% of the L_{sw}). Based on this analysis, therefore, a local swash correction factor of 0.15 L_{sw} was found. Application of this correction to the MSV method shorelines resulted in a reduction of the RMS difference between 0.5-min MSV shorelines and GPS shorelines by -10.1%.

The resulting error made on shoreline-position video estimation has various origins. Our results show that a substantial part of the error can be corrected based on swash length. Another important source of error can be attributed to bad image quality. This can be overcome by a preliminary quality check and rejecting poor-quality images. This is part of the first step in the MSV method, similarly to other automatic (Uunka, Wijnberg, and Morelissen, 2009) or manual (Aarninkhof *et al.*, 2003) methods. Nevertheless, “nonphysical” errors could be largely reduced using a statistical approach. The principle is to establish long-term statistics of shoreline dynamics and to

compare them with individual variation. For instance, 1 and 7 m/d of average and maximum variation values, respectively, were found at a nearby beach of Truc Vert equipped with a permanent video system over a 2-y period (Almar, 2009). Hence, one way to correct shoreline databases would be to detect and remove shorelines associated with excessive day-to-day variations by comparing those values with the statistical values expected.

Other sources of inaccuracy are inherent to the video system set up and are constant over time: image resolution, distortion and rectification, and camera distance and view angle. However, these inaccuracies have an order of value of O (1 cm to 1 m) smaller than other errors previously described.

CONCLUSIONS

The video estimation of shoreline position at beaches with high wave energy and large temporal and spatial variability and meso-macro tides has remained, to date, a challenging task. In this study, a combination of video imaging and concurrent GPS tracking was adopted to detect complex nonmonotonic shorelines at Truc Vert beach, France, a typical meso-macro tidal, high wave-energy beach with large temporal and spatial shoreline variations.

A new video method (the Minimum Shoreline Variability [MSV] method) has been developed that is capable of differentiating between the water/sand interface and dry sand/wet sand interface and preferentially picks the former as the shoreline. More confidence can be placed on shorelines detected using short-time averaged video images (<2 min) compared with those obtained using the traditional long-time averaging images (10 min).

The MSV error is linearly correlated to local swash length, which has high spatiotemporal variability. Contrary to previous unique swash-length estimations based on offshore wave height and beach characteristics, here, the local swash length is estimated *via* video images. A correction ($0.15 \times$ the local swash length) is suggested. Application of this correction results in a substantial (10%) improvement of the accuracy of MSV shorelines. Combining the use of short 0.5-min averaging of images and the local swash correction factor allows a 30% error reduction relative to the initial shoreline detection method. The cross-shore accuracy of corrected MSV shorelines is up to 1.2 m, which is an accuracy that is generally seen as satisfactory, even at monotonous microtidal low-energy beaches.

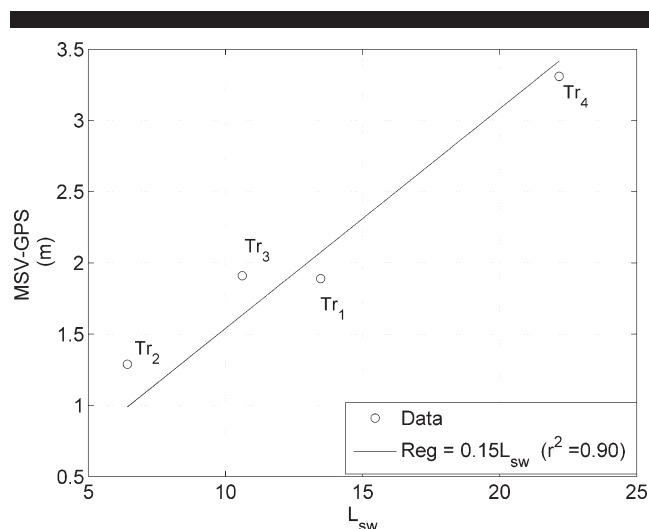


Figure 9. The MSV-GPS difference plotted against the measured swash excursion length (L_{sw}). The MSV data are from 0.5-min time-exposure images and corresponds to 120 shoreline estimations averaged for the four swash tracks ($Tr_{1,2,3,4}$). The regression line shows the linear relationship between the error and swash length.

ACKNOWLEDGMENTS

The ECORS experiment and TVB video system were supported financially by the French “Service Hydrographique et Oceanographique de la Marine” (SHOM). The PhD thesis of R.A. was funded by the French “Délégation Générale de l’Armement” (DGA), and part of work was supported by PUC-Escuela de Ingenieria and FONDECYT through project 3110030. The authors wish to thank D. Corman (SHOM) and IHE-UNESCO MsC students, T. Duong, N. Garae, D. Merli, A. Mokhtar, M. Nguyen, F. Novico, and K. Ofori for their assistance in the field.

LITERATURE CITED

- Aarninkhof, S.G.J.; Turner, I.L.; Dronkers, T.D.T.; Caljouw, M., and Nipius, L., 2003. A video-based technique for mapping intertidal beach bathymetry. *Coastal Engineering*, 49(4), 275–289.
- Almar, R., 2009. High Frequency Nearshore Hydro-Morphodynamics from Video Imagery. Bordeaux, France: Université de Bordeaux, doctoral thesis [in French].
- Almar, R.; Castelle, B.; Ruessink, G.; Sénéchal, N.; Bonneton, P., and Marieu, V. 2010 Two- and three-dimensional double-sandbar system behaviour under intense wave forcing and a meso-macro tidal range. *Continental Shelf Res*, 30(7), 781–792.
- Boak, E.H. and Turner, I.L., 2005. Shoreline definition and detection: a review. *Journal of Coastal Research*, 21(4), 688–703.
- Bryan, K.R.; Smith, R.K., and Ovenden, R., 2003. The use of video camera to assess beach volume change between April and June 2001 at Tairua, New Zealand. *Coasts and Ports '03: Proceedings of the 16th Australasian Coastal and Ocean Engineering conference and the 97th Australasian Port and Harbour Conference* (Auckland, New Zealand, IPENZ), paper 19.
- Butel, R.; Dupuis, H., and Bonneton, P., 2002. Spatial variability of wave conditions on the French Atlantic coast using in-situ data. In: Cooper, J.A.G. and Jackson, D.W.T. (eds.), *The 7th International Coastal Symposium (ICS 2002, Northern Ireland)*, Journal of Coastal Research, Special Issue No. 36, pp. 96–108.
- Castelle, B.; Bonneton, P.; Dupuis, H., and Sénéchal, N., 2007. Double bar beach dynamics on the high-energy meso-macrotidal French Aquitanian coast: a review. *Marine Geology*, 245, 141–159.
- Castelle, B.; Turner, I.L.; Bertin, X., and Tomlinson, R., 2009. Beach nourishments at Coolangatta Bay over the period 1987–2005: impacts and lessons. *Coastal Engineering*, 56(9), 940–950.
- Coco, G.; Bryan, K., and Payne, G., 2004. The next era for cam-era. *Coastal News*.
- Davidson, M.; Van Koningsveld, M.; De Kruif, A.; Rawson, J.; Holman, R.; Lamberti, A.; Medina, R.; Kroon, A., and Aarninkhof, S., 2007. The coast view project: developing video-derived coastal state indicators in support of coastal zone management. *Coastal Engineering*, 54, 463–475.
- Holland, K.T.; Holman, R.A.; Lippmann, T.C.; Stanley, J., and Plant, N., 1997. Practical use of video imagery in nearshore oceanographic field studies. *Oceanic Engineering*, 22(1), 81–92.
- Holman, R.A. and Stanley, J., 2007. The history and technical capabilities of Argus. *Coastal Engineering*, 54(6–7), 477–491.
- Jiménez, J.A.; Osorio, A.; Marino-Tapia, I.; Davidson, M.; Medina, R.; Kroon, A.; Archetti, R.; Ciavola, P., and Aarninkhof, S.G.J., 2007. Beach recreation planning using video-derived coastal state indicators. *Coastal Engineering*, 54, 507–521.
- Kroon, A.; Davidson, M.A.; Aarninkhof, S.G.J.; Archetti, R.; Armaroli, C.; Gonzalez, M.; Medri, S.; Osorio, A.; Aagaard, T.; Holman, R.A., and Spanhoff, R., 2007. Application of remote sensing video systems to coastline management problems. *Coastal Engineering*, 54, 493–505.
- Lafon, V.; Dupuis, H.; Howa, H., and Froidefond, J.-M., 2002. Determining ridge and runnel longshore migration rate using spot imagery. *Oceanologica Acta*, 25, 149–158.
- Parisot, J.P.; Capo, S.; Bujan, S.; Sénéchal, N.; Moreau, J.; Réjas, A.; Hanquiez, V.; Almar, R.; Marieu, V.; Castelle, B.; Gaunet, J.; Gluard, L.; George, I.; Nahon, A.; Dehouck, A.; Certain, R.; Gervais, M.; Barthe, P.; Ardhuin, F.; Le Gall, F.; Bernardi, P.J.; Le Roy, R.; Pedreros, R.; Delattre, M., and MacMahan, J., 2008. Sedimentary processes and morphodynamics of sandy beaches on short time response. In: da Silva, C.P. (ed.). Treatment of topographic and bathymetric data acquired at the Truc-Vert Beach (SW France) during the ECORS mission. *The 10th International Coastal Symposium (ICS 2009, Lisbon, Portugal)*, Volume 2, Journal of Coastal Research, Special Issue No. 56, pp. 1786–1790.
- Pedreros, R.; Howa, H.L., and Michel, D., 1996. Application of grain size trend analysis for the determination of sediment transport pathways in intertidal areas. *Marine Geology*, 135, 35–49.
- Plant, N.G. and Holman, R.A., 1997. Intertidal beach profile estimation using video images. *Marine Geology*, 140(1–2), 1–24.
- Plant, N.G.; Aarninkhof, S.G.; Turner, I.L., and Kingston, K.S., 2007. The performance of shoreline detection models applied to video imagery. *Journal of Coastal Research*, 23(3), 658–670.
- Rihouey, D.; Dugor, J.; Dailloux, D., and Morichon, D., 2009. Application of remote sensing video systems to coastal defence monitoring. In: da Silva, C.P. (ed.). *The 10th International Coastal Symposium (ICS 2009, Lisbon, Portugal)*, Volume 2, Journal of Coastal Research, Special Issue No. 56, pp. 1582–1586.
- Ruessink, B.G., 1998. The temporal and spatial variability of infragravity waves in a barred nearshore zone. *Continental Shelf Research*, 18, 585–605.
- Sénéchal, N. and Ardhuin, F. 2008. ECORS Truc Vert’ 08: a multi-institutional international nearshore field experiment. In: *American Geophysical Union Fall Meeting 2008* (San Francisco, California, AGU), Abstract OS12B-02.
- Silva, A.N.; Taborda, R.; Catalão, J., and Freire, P., 2009. DTM extraction using video-monitoring techniques: application to a fetch limited beach. In: da Silva, C.P. (ed.). *The 10th International Coastal Symposium (ICS 2009, Lisbon, Portugal)*, Volume 2, Journal of Coastal Research, Special Issue No. 56, pp. 203–207.
- Smith, R.K., and Bryan, K.R., 2007. Monitoring beach face volume with a combination of intermittent profiling and video imagery. *Journal of Coastal Research*, 23(4), 892–898.
- Smit, M.W.J.; Aarninkhof, S.G.J.; Wijnberg, K.M.; González, M.; Kingston, K.S.; Southgate, H.N.; Ruessink, B.G.; Holman, R.A.; Siegle, E.; Davidson, M., and Medina, R., 2007. The role of video imagery in predicting daily to monthly coastal evolution. *Coastal Engineering*, 54(6–7), 539–553.
- Turner, I.; Leyden, V.; Symonds, G.; McGrath, J.; Jackson, A.; Jancar, T.; Aarninkhof, S.G.J., and Elshoff, I.E., 2001. Comparison of observed and predicted coastline changes at the gold coast artificial (surfing) reef, Sydney, Australia. In: Edge, B.L. (ed.), *Coastal Engineering 2000: Proceeding of the 27th International Conference on Coastal Engineering* (Sydney, Australia, ASCE), pp. 1836–1847.
- Uunka, L.; Wijnberg, K.M., and Morelissen, R. 2009. Automated mapping of the intertidal beach bathymetry from video images. *Coastal Engineering*, 57(4), 461–469.
- Wright, L.D. and Short, A.D., 1984. Morphodynamic variability of surf zones and beaches: a synthesis. *Marine Geology*, 56, 93–118.